ESN Publishing

Contents lists available at ESN Publishing Journals

International Journal of Digital Technology Driven Engineering

journal homepage: https://journals.esn-press.com/ijdtde



Research Article

A Mixed Nonlinear Complementarity Formulation for Second-Order Frictional Grasping with Multifingered Robot Grippers

Ahmad M. Al-Fahed Nuseirat[1,*]

[1] *Independent Researcher, P.O. Box 1234, 11821 Amman, Jordan*

ARTICLE INFO

Article type:
Research Article

Keywords:
Frictional grasping
Second-order grasp analysis
Mixed complementarity problem
Contact mechanics
Equilibrium feasibility
Multi-fingered robot grippers

ABSTRACT

This paper presents a mixed nonlinear complementarity problem (MNCP) formulation for an object grasped by a frictional multifingered robot gripper, in which the contact kinematics are expanded to second order. The proposed approach extends the first-order contact kinematics used in prior complementarity formulations of frictional grasping by introducing a quadratic term, $\mathbf{\Gamma}(\delta\boldsymbol{\eta}, \delta\boldsymbol{\eta})$, which captures curvature-dependent geometric effects that are absent from a linearized contact description.

The formulation accounts for unilateral hard-finger contacts with isotropic or anisotropic Coulomb friction, expressed through complementarity conditions, and is solved using a semismooth Newton method based on the Fischer–Burmeister function.

Numerical examples demonstrate the influence of the second-order geometric terms on the contact-force distribution and on the available friction margin. An analytically solvable benchmark reproduces the closed-form solution to machine precision, providing an independent verification of the equilibrium, friction, and complementarity implementation.

1 Introduction

Robotic grasping and manipulation involve the interaction of robotic fingers with objects through unilateral and frictional contacts. The mechanics of these interactions determine whether a grasp can balance an external wrench, resist disturbances, and maintain contact without undesired slip. Classical studies have established fundamental concepts such as force closure, grasp stability, contact-force distribution, and the role of friction in determining grasp feasibility [1, 2]. More recent surveys have placed these concepts within the broader development of analytical and computational grasp-synthesis methods for autonomous multifingered robotic hands [3]. However, the mechanical behavior of frictional contact is inherently nonsmooth: contacts may open or close, and friction may transition between sticking and sliding states. Capturing these transitions within a mathematically tractable framework remains a central challenge.

Several mathematical approaches have been developed for analyzing multifingered grasping. Grasp capability can be formulated as a constrained optimization problem involving object equilibrium, joint torque limits, contact-force constraints, and prevention of fingertip slip [4]. Optimization-based formulations have also been used to determine grasping forces while accounting for finger deformability and object-positioning constraints [5], whereas grasp-wrench-set approaches provide efficient methods for contact-force distribution [6]. These developments illustrate the importance of simultaneously accounting for equilibrium, contact

∗ Corresponding author. E-mail address: anuseirat@gmail.com.
Received 4 October 2026; Revised 24 October 2026; Accepted 25 October 2026
© 2026 The Authors. Published by European Scientific Network Publishing.
This is an open access article under the CC BY 4.0 license (https://creativecommons.org/licenses/by/4.0/).

constraints, friction, and the mechanical characteristics of the multifingered robotic gripper. While these optimization formulations effectively handle many aspects of grasp analysis, they do not explicitly capture the nonsmooth character of contact transitions, which is better addressed through complementarity-based approaches.

Frictional contact is inherently nonsmooth. Contact points may open or close, while closed contacts may undergo sticking or sliding depending on whether the friction limit is active. Such mutually exclusive contact states cannot, in general, be represented solely by globally smooth equality relations and are naturally described through inequalities, variational principles, and complementarity conditions.

These features belong to the broader framework of nonsmooth mechanics, in which unilateral contact, dry friction, and nonclassical constitutive relations are treated using inequality-based formulations [7, 8, 9]. Panagiotopoulos established a general framework for inequality problems in mechanics encompassing variational inequalities, nonconvex and multivalued mechanical problems, and frictional contact, which was subsequently extended to nonsmooth systems by Moreau and Panagiotopoulos [7, 8].

Complementarity methods provide a particularly useful finite-dimensional representation of unilateral and frictional contact conditions. The unilateral condition can be expressed through complementarity between the normal gap and the normal contact force, while frictional conditions combine inequality constraints with slip and friction-limit relations. Complementarity formulations have consequently been employed in contact mechanics and multibody systems with Coulomb friction [10, 11, 12, 13]. Within robotic grasping, they have been developed within both linear and nonlinear frameworks. Early optimization-based approaches to grasping included LP formulations for form-closure testing [14] and LCP formulations for multifingered frictional grippers with polyhedral friction cones [15, 16], whereas later NCP-based formulations retained the exact nonlinear friction boundary [17, 18]. Complementarity methods have also been applied to related problems in legged locomotion and multi-arm manipulation [19, 9]. These formulations provide a systematic means of determining contact states and forces without prescribing the active contact set a priori.

Second-order contact kinematics have their origins in the classical differential-geometric formulation of the contact equations for rigid bodies [20, 21]. These formulations describe the motion of the contact point and the evolution of the local contact frame in terms of the surface geometry and the relative motion of the bodies, and they provide the natural framework for extending first-order complementarity descriptions of grasping to second order. In the context of grasping, these kinematic relations determine how contact points, normal directions, and tangent frames evolve as the finger and object move relative to each other. To first order, this evolution is captured by linear relations; to second order, curvature-dependent quadratic terms appear.

Despite these developments, second-order contact geometry and complementarity-based frictional grasping have largely been treated through separate modeling viewpoints. Existing complementarity formulations for multifingered grasping are predominantly based on first-order contact kinematics, whereas second-order grasp analyses have principally focused on mobility, stability, and curvature-dependent geometric properties [22, 23, 24]. Consequently, there remains a need for a formulation that retains the unilateral and nonsmooth character of frictional contact while explicitly incorporating second-order contact kinematics. For example, variations in the local contact frame and curvature-induced changes in the normal direction are neglected in first-order models, which may affect the predicted contact-force distribution when the relative motion is small but finite.

The present work extends the first-order NCP formulation of Al-Fahed Nuseirat and Stavroulakis [17] by incorporating second-order contact kinematics, while retaining the nonlinear friction treatment of [17]. Specifically, the contact kinematics are expanded about an equilibrium configuration, giving the quadratic correction $\mathbf{\Gamma}(\delta\boldsymbol{\eta}, \delta\boldsymbol{\eta})$, where $\delta\boldsymbol{\eta}$ denotes the infinitesimal relative motion of the contacting bodies. This term accounts for second-order geometric effects associated with the local contact geometry and is incorporated directly into the contact compatibility relations. The resulting formulation therefore retains unilateral contact and nonlinear friction conditions while introducing second-order geometric information that is absent from the corresponding first-order model.

The grasping problem is formulated as a mixed nonlinear complementarity problem (MNCP) comprising object equilibrium, finger kinematics and compliance relations, unilateral contact conditions, nonlinear friction constraints, and second-order contact compatibility. The formulation considers hard-finger contacts and allows both isotropic and anisotropic translational friction. The resulting nonlinear complementarity system is solved using a semismooth Newton method based on the Fischer–Burmeister function [25, 26, 27].

The main contributions of this work are summarized as follows:

- A second-order MNCP formulation is developed that extends prior first-order complementarity descriptions of frictional grasping by incorporating quadratic contact-kinematics corrections.
- The second variation of the nonlinear contact mapping is incorporated explicitly into the normal and frictional contact compatibility relations, thereby accounting for curvature-dependent geometric effects.
- Hard–finger contact with isotropic and anisotropic translational friction is incorporated within the proposed second-order complementarity framework.
- A semismooth Newton solver based on the Fischer–Burmeister function is adapted to the second–order MNCP, and its convergence from well-conditioned initial guesses is demonstrated numerically.

The remainder of the paper is organized as follows. Section 2 presents the grasp configuration, equilibrium conditions, and frictional contact model. Section 3 develops the first- and second-order contact kinematics. Section 4 assembles the governing relations into the mixed nonlinear complementarity formulation. Section 5 presents the numerical solution procedure. Section 6 provides numerical examples and compares the first- and second-order predictions. Finally, Section 7 summarizes the main conclusions.

2 Problem Formulation

2.1 Contact Coordinate Systems

Consider an object grasped by n articulated fingers. Define a reference frame O_p attached to the palm of the gripper and a body-fixed coordinate system O_b located at the center of mass of the object. The geometric configuration of the multifingered grasping system and the associated reference frames are illustrated in Figure 1.

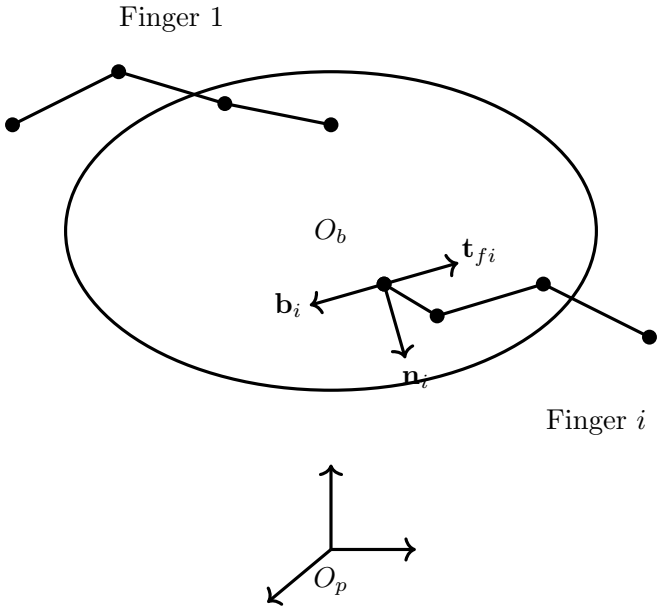


Figure 1: Geometric configuration of the multifingered grasping system, showing the palm frame O_p, the object body frame O_b, and the local contact frames O_{bi} and O_{li} at contact i.

At each contact point i, we define:

- a local object frame O_{bi} attached to the object surface,
- a local finger frame O_{li} attached to the fingertip.

At contact, the origins of O_{bi} and O_{li} coincide. The local x-axis is aligned with the outward normal to the contact surface, and the y- and z-axes span the tangent plane, chosen to form a right-handed orthonormal frame with the x-axis.

This work builds upon the grasping models in [17] to develop a genuine second-order formulation. Unlike the first-order model, which only considers the direction of contact at the contact points of the object being held, the second-order model incorporates the second-order kinematics of contact through a quadratic approximation of the gap functions for each contact point. In addition, the Coulomb friction law remains

in its nonlinear form without any assumption of linearity.

2.2 Equilibrium Equations

For an object grasped by n articulated fingers, its equilibrium equations can be formulated as

$$\mathbf{G}\mathbf{f} = \mathbf{P}, \tag{1}$$

where

$$\mathbf{G} = \begin{bmatrix} \mathbf{G}_n \mid \mathbf{G}_t \end{bmatrix}, \qquad \mathbf{f} = \begin{bmatrix} \mathbf{f}_n \\ \mathbf{f}_t \end{bmatrix},$$

$\mathbf{f}$ is the vector of contact forces, $\mathbf{f}_n = [f_{n1}, f_{n2}, \ldots, f_{nn}]^T$ is the vector of the normal forces exerted by the fingers on the object, $\mathbf{f}_t = [f_{t11}, f_{t12}, f_{t21}, f_{t22}, \ldots, f_{tn1}, f_{tn2}]^T$ is the vector of tangential friction forces for hard-finger contact, and $\mathbf{P}$ is the vector of external generalized forces acting on the object.

The matrix $\mathbf{G} = [\mathbf{G}_n \mid \mathbf{G}_t]$ is the grasp equilibrium matrix, with $\mathbf{G} \in \mathbb{R}^{m \times 3n}$ for spatial hard-finger contact, where m is the number of independent components of the external wrench ($m = 6$ for spatial grasping and $m = 3$ for planar grasping). The matrix is constructed using the contact-wrench basis and the corresponding coordinate transformations, following [17]. The matrices $\mathbf{G}_n$ and $\mathbf{G}_t$ represent the normal and tangential grasp maps, respectively, which transform local contact forces into generalized forces acting on the rigid body. The equilibrium equations are obtained by assembling the contributions of all contact forces and balancing them against the external load vector $\mathbf{P}$.

To preserve the complementarity structure of the formulation, the tangential friction force vector $\mathbf{f}_t$ is decomposed into nonnegative positive and negative parts,

$$\mathbf{f}_t = \mathbf{f}_t^+ - \mathbf{f}_t^-, \qquad \mathbf{f}_t^+ \geq 0, \qquad \mathbf{f}_t^- \geq 0, \tag{2}$$

a decomposition that will be used in the complementarity formulation developed in Section 4.

3 Contact Kinematics

In this section, the kinematics of the articulated multifingered gripper in contact with a rigid object are formulated. The methodology follows the approach introduced by [15] and [28], extended here to include second-order contact kinematics at the interface between the articulated fingers and the object.

The kinematics of a grasp configuration using a multifingered gripper can be described by a first-order approximation that relates the object's rigid-body motion to the motion of each gripper finger and the relative motion at all points of contact. However, the first-order approximation does not account for geometric nonlinearities that arise from the curvature of the surfaces being grasped and variations in the alignment of the local contact frames. To account for these effects, a second-order kinematic representation of the contact kinematics is developed below.

3.1 Kinematic Variables

The rigid-body displacement vector describes the motion of the grasped object:

$$\mathbf{u}_o = \begin{bmatrix} \mathbf{u}_b \\ \boldsymbol{\omega}_b \end{bmatrix}, \tag{3}$$

where $\mathbf{u}_b \in \mathbb{R}^3$ and $\boldsymbol{\omega}_b \in \mathbb{R}^3$ denote, respectively, the translational displacement and the infinitesimal rotational displacement of the rigid object about the reference configuration. The vector $\boldsymbol{\omega}_b$ is an incremental rotation vector used in the local kinematic description rather than a global parameterization of finite orientation. This representation follows the treatment of rigid-body displacements and rotations in unilateral contact problems given in [28].

The vector of finger-joint displacements, including revolute and prismatic joint coordinates as appropriate, is denoted by

$$\mathbf{dq} \in \mathbb{R}^{n_q}, \tag{4}$$

where n_q is the total number of joint coordinates of the multifingered gripper. The quantities $\mathbf{u}_b$, $\boldsymbol{\omega}_b$, and $\mathbf{dq}$ describe the first-order motion of the object–hand system.

3.2 First-Order Contact Kinematics

Let $\mathbf{y}$ denote the relative displacement at the contacts, partitioned into normal and tangential components:

$$\mathbf{y} = \begin{bmatrix} \mathbf{y}_n \\ \mathbf{y}_t \end{bmatrix}. \tag{5}$$

Here, $\mathbf{y}_n$ denotes the normal relative displacement at the potential contact points. Its component y_{ni} may be interpreted as the normal gap function for the ith finger–object pair: $y_{ni} > 0$ corresponds to an open contact, whereas $y_{ni} = 0$ corresponds to an active unilateral contact. The vector $\mathbf{y}_t$ denotes the relative tangential displacement at the corresponding contact points, expressed in the local tangent coordinates. These quantities are defined relative to the reference configuration and include the initial gaps or offsets introduced below.

The relative displacement arises from three physical contributions:

- the rigid-body motion of the object,
- the joint motion of the fingers,
- the elastic deformation of the fingertips and the hand structure.

Using the principle of virtual work, the contribution of the rigid-body motion is given by

$$\mathbf{u}_{on} = -\mathbf{G}_n^T \mathbf{u}_o, \qquad \mathbf{u}_{ot} = -\mathbf{G}_t^T \mathbf{u}_o, \tag{6}$$

where $\mathbf{G}_n$ and $\mathbf{G}_t$ are the normal and tangential grasp matrices, respectively.

The contribution of the joint motion is expressed as

$$\mathbf{u}_n^j = \mathbf{J}_n \mathbf{dq}, \qquad \mathbf{u}_t^j = \mathbf{J}_t \mathbf{dq}, \tag{7}$$

where $\mathbf{J}_n$ and $\mathbf{J}_t$ are the corresponding Jacobian matrices.

The elastic deformation of the fingertips is modeled through linear compliance relations:

$$\mathbf{u}_n^e = \mathbf{F}_{nn}\mathbf{f}_n + \mathbf{F}_{nt}\mathbf{f}_t, \qquad \mathbf{u}_t^e = \mathbf{F}_{tn}\mathbf{f}_n + \mathbf{F}_{tt}\mathbf{f}_t, \tag{8}$$

where $\mathbf{f}_n$ and $\mathbf{f}_t$ denote the normal and tangential contact forces. The compliance matrices have dimensions $\mathbf{F}_{nn} \in \mathbb{R}^{n\times n}$, $\mathbf{F}_{nt} \in \mathbb{R}^{n\times 2n}$, $\mathbf{F}_{tn} \in \mathbb{R}^{2n\times n}$, and $\mathbf{F}_{tt} \in \mathbb{R}^{2n\times 2n}$, reflecting the partition of the contact force into normal and tangential components.

Accordingly, the first-order relative displacements are written as

$$\mathbf{y}_n = \mathbf{u}_n^e + \mathbf{u}_n^j - \mathbf{u}_{on} + \mathbf{c}_n, \tag{9}$$

$$\mathbf{y}_t = \mathbf{u}_t^e + \mathbf{u}_t^j - \mathbf{u}_{ot} + \mathbf{c}_t, \tag{10}$$

where $\mathbf{c}_n$ represents the initial normal gaps and $\mathbf{c}_t$ the initial tangential offsets with respect to the reference configuration.

3.3 Constraints Introduced by Finger Joints

Joint variables (revolute and prismatic joints) are associated with joint actuators (torques) and design parameters. The relationship between fingertip position components and joint motion is expressed as

$$\begin{bmatrix} \mathbf{u}_n^j \\ \mathbf{u}_t^j \end{bmatrix} = \begin{bmatrix} \mathbf{J}_n \\ \mathbf{J}_t \end{bmatrix} \mathbf{dq}, \tag{11}$$

where

$$\begin{aligned} \mathbf{J}_n &= \operatorname{diag}\left[\mathbf{N}_n\mathbf{J}_1, \mathbf{N}_n\mathbf{J}_2, \ldots, \mathbf{N}_n\mathbf{J}_{n_f}\right], \\ \mathbf{J}_t &= \operatorname{diag}\left[\mathbf{N}_t\mathbf{J}_1, \mathbf{N}_t\mathbf{J}_2, \ldots, \mathbf{N}_t\mathbf{J}_{n_f}\right], \\ \mathbf{dq} &= \left[\mathbf{dq}_1, \mathbf{dq}_2, \ldots, \mathbf{dq}_{n_f}\right], \end{aligned}$$

n_f is the number of fingers, $\mathbf{dq}_i$ denotes the vector of joint motions of the ith finger, and $\mathbf{J}_i \in \mathbb{R}^{6\times n_{q,i}}$ is the Jacobian matrix of the ith finger's fingertip, mapping its joint velocities to its spatial velocity, with $n_{q,i}$ the number of joints of the ith finger. The constraint matrices $\mathbf{N}_n$ and $\mathbf{N}_t$ extract the normal and tangential components of the fingertip velocity and have the form

$$\mathbf{N}_n = \begin{bmatrix} 1 & 0 & 0 & 0 & 0 & 0 \end{bmatrix},$$
$$\mathbf{N}_t = \begin{bmatrix} 0 & 1 & 0 & 0 & 0 & 0 \\ 0 & 0 & 1 & 0 & 0 & 0 \end{bmatrix}.$$

Applying the principle of virtual work, the joint torques are related to the contact forces by

$$\boldsymbol{\tau} = \mathbf{J}_n^T \mathbf{f}_n + \mathbf{J}_t^T \mathbf{f}_t, \tag{12}$$

where $\boldsymbol{\tau} = [\boldsymbol{\tau}_1, \boldsymbol{\tau}_2, \ldots, \boldsymbol{\tau}_{n_f}]^T$ and $\boldsymbol{\tau}_i$ is the vector of joint torques of the ith finger.

Assuming that the joints behave as linear torsional (respectively, linear translational) springs, with stiffness characterized by the compliance matrix

$$\mathbf{F}_j = \operatorname{diag}[\mathbf{F}_{j1}, \mathbf{F}_{j2}, \ldots, \mathbf{F}_{jn_f}], \tag{13}$$

the joint displacements are related to the joint torques by

$$\mathbf{dq} = \mathbf{F}_j \boldsymbol{\tau}, \tag{14}$$

where $\mathbf{F}_{ji} \in \mathbb{R}^{n_{q,i}\times n_{q,i}}$ is a diagonal matrix whose entries are the compliances of the springs of the ith finger. Substituting (14) into (11), we obtain

$$\begin{bmatrix} \mathbf{u}_n^j \\ \mathbf{u}_t^j \end{bmatrix} = \begin{bmatrix} \mathbf{J}_n \\ \mathbf{J}_t \end{bmatrix} \mathbf{F}_j \boldsymbol{\tau}. \tag{15}$$

Finally, substituting (12) into (15), the joint contribution to the relative displacement can be expressed as a compliance relation in terms of the contact forces,

$$\begin{bmatrix} \mathbf{u}_n^j \\ \mathbf{u}_t^j \end{bmatrix} = \begin{bmatrix} \mathbf{J}_n \mathbf{F}_j \mathbf{J}_n^T & \mathbf{J}_n \mathbf{F}_j \mathbf{J}_t^T \\ \mathbf{J}_t \mathbf{F}_j \mathbf{J}_n^T & \mathbf{J}_t \mathbf{F}_j \mathbf{J}_t^T \end{bmatrix} \begin{bmatrix} \mathbf{f}_n \\ \mathbf{f}_t \end{bmatrix}. \tag{16}$$

3.4 Friction Conditions

Frictional contact problems of this type can be naturally formulated within the framework of variational inequalities and complementarity theory [7]. Within this framework, the ith finger exerts a tangential force on the object within a friction cone based on Coulomb's dry friction law. For a general formulation of the hard-finger contact, an orthotropic friction law is adopted, in which the friction coefficients along the two principal tangential directions may differ. This is relevant for materials with directional surface properties and reduces to isotropic friction when the two coefficients are equal. The friction function is defined as

$$\psi_i(\mathbf{f}_i) = f_{ni}^2 - \frac{f_{ti1}^2}{\mu_{i1}^2} - \frac{f_{ti2}^2}{\mu_{i2}^2}, \tag{17}$$

where f_{ni} is the normal force, f_{ti1} and f_{ti2} are the tangential force components, and μ_{i1}, μ_{i2} are the orthotropic friction coefficients of contact i.

The friction admissibility condition is then

$$\psi_i(\mathbf{f}_i) \geq 0. \tag{18}$$

When the friction constraint is active ($\psi_i = 0$), the contact is sliding and the tangential slip components are expressed through a nonnegative multiplier λ_i as

$$y_{ti1} = -\lambda_i \frac{f_{ti1}}{\mu_{i1}^2}, \qquad y_{ti2} = -\lambda_i \frac{f_{ti2}}{\mu_{i2}^2}, \tag{19}$$

where the negative sign indicates that the slip direction opposes the tangential force, consistent with Coulomb friction. When the friction constraint is strictly satisfied ($\psi_i > 0$), the contact is sticking and $\lambda_i = 0$. The isotropic friction law is a particular case of the orthotropic law (17), obtained when $\mu_{i1} = \mu_{i2} = \mu_i$.

3.5 Second-Order Expansion

The first-order contact relations describe relative contact motion through a linearization about a reference configuration. For curved contacting surfaces, however, variations in the contact geometry and local coordinate frames may introduce quadratic contributions that are not represented by the first-order approximation. This subsection develops the second-order contact relations using the Hessian of a nonlinear contact mapping and illustrates the resulting geometric terms for spherical contacts.

3.5.1 Nonlinear Contact Mapping

Let $\boldsymbol{\eta}$ denote the generalized configuration of the object–hand system, including the object pose and finger-joint coordinates. At contact i, define the nonlinear relative-displacement mapping

$$\boldsymbol{\phi}_i(\boldsymbol{\eta}) = \mathbf{R}_{ci}^T(\boldsymbol{\eta}) \left[\mathbf{p}_{fi}(\boldsymbol{\eta}) - \mathbf{p}_{oi}(\boldsymbol{\eta})\right], \tag{20}$$

where $\mathbf{p}_{fi}$ and $\mathbf{p}_{oi}$ are the positions of the associated fingertip and object material points, and $\mathbf{R}_{ci}$ defines the local contact frame. The mapping provides the relative displacement resolved along the local normal and two tangential directions.

The positions and contact frame may depend on the generalized configuration. Consequently, differentiation of $\boldsymbol{\phi}_i$ accounts for the kinematic dependence of the contact coordinates on object and finger motion.

For contact models in which the active contact points migrate over the surfaces, the mapping must additionally specify the contact-point parameters and their evolution. Such migration is not implied by the fixed-material-point mapping in (20).

3.5.2 Second-Order Taylor Expansion

Consider a perturbation about a reference configuration $\boldsymbol{\eta}^*$, expressed in local generalized coordinates as

$$\delta\boldsymbol{\eta} = \begin{bmatrix} \delta\mathbf{u}_b \\ \delta\boldsymbol{\omega}_b \\ \delta\mathbf{q} \end{bmatrix}, \tag{21}$$

where $\delta\mathbf{u}_b$ and $\delta\boldsymbol{\omega}_b$ represent object translation and rotation, respectively, and $\delta\mathbf{q}$ represents finger-joint perturbations.

Assuming that the contact mapping is twice continuously differentiable near $\boldsymbol{\eta}^*$, its Taylor expansion is

$$\begin{aligned} \boldsymbol{\phi}(\boldsymbol{\eta}^* + \delta\boldsymbol{\eta}) = \boldsymbol{\phi}(\boldsymbol{\eta}^*) + D\boldsymbol{\phi}(\boldsymbol{\eta}^*)\delta\boldsymbol{\eta} \\ + \frac{1}{2}\boldsymbol{\Gamma}(\delta\boldsymbol{\eta}, \delta\boldsymbol{\eta}) + o(\|\delta\boldsymbol{\eta}\|^2). \end{aligned} \tag{22}$$

Here, $D\boldsymbol{\phi}$ is the Jacobian of the contact mapping, while $\boldsymbol{\Gamma}$ denotes its second directional variation.

For each scalar component $\phi_{i,k}$, define

$$\mathbf{H}_{i,k} = \nabla_{\boldsymbol{\eta}}^2 \phi_{i,k}(\boldsymbol{\eta}^*), \qquad k = 1, 2, 3. \tag{23}$$

The second-order correction at contact i is then

$$\boldsymbol{\Gamma}_i = \begin{bmatrix} \delta\boldsymbol{\eta}^T \mathbf{H}_{i,1} \delta\boldsymbol{\eta} \\ \delta\boldsymbol{\eta}^T \mathbf{H}_{i,2} \delta\boldsymbol{\eta} \\ \delta\boldsymbol{\eta}^T \mathbf{H}_{i,3} \delta\boldsymbol{\eta} \end{bmatrix}. \tag{24}$$

The Hessians are evaluated at the reference configuration and are therefore fixed within the local quadratic approximation. They may contain pure and mixed derivatives associated with object translation, rotation, and finger-joint motion.

The correction $\boldsymbol{\Gamma}_i$ has the dimensions of displacement. It represents a geometric contribution to the contact kinematics and should not be interpreted as a contact stiffness.

3.5.3 Second-Order Contact Compatibility

The second-order correction is partitioned into normal and tangential components according to the ordering of the local contact coordinates:

$$\mathbf{\Gamma} = \begin{bmatrix} \mathbf{\Gamma}_n \\ \mathbf{\Gamma}_t \end{bmatrix}, \tag{25}$$

where $\mathbf{\Gamma}_n$ contains one component per contact and $\mathbf{\Gamma}_t$ contains two components per contact.

The first-order normal and tangential compatibility relations are consequently extended to

$$\mathbf{y}_n = \mathbf{u}_n^e + \mathbf{u}_n^j - \mathbf{u}_{on} + \mathbf{c}_n + \frac{1}{2}\mathbf{\Gamma}_n, \tag{26}$$

$$\mathbf{y}_t = \mathbf{u}_t^e + \mathbf{u}_t^j - \mathbf{u}_{ot} + \mathbf{c}_t + \frac{1}{2}\mathbf{\Gamma}_t. \tag{27}$$

The first-order model is recovered by setting $\mathbf{\Gamma}_n = \mathbf{0}$ and $\mathbf{\Gamma}_t = \mathbf{0}$.

The normal correction describes the quadratic variation of the normal contact coordinate, whereas the tangential correction describes the corresponding variation of the two tangential coordinates.

In the numerical implementation, the second-order corrections are evaluated for prescribed small perturbations and treated as fixed geometric terms during the MNCP solution.

3.5.4 Illustrative Example: Spherical Contact Geometry

The differential geometry of contacting surfaces and its application to robotic grasping have been investigated by Montana [20]. Rigid-body rotations may be represented using exponential coordinates, as described by Murray et al. [29].

Consider a spherical object of radius R grasped by spherical fingertips of radius R_f. At contact i, let $\mathbf{r}_i$ be the vector from the object center to the reference object contact point. Define the orthonormal contact frame

$$\mathbf{C}_i = \begin{bmatrix} \mathbf{n}_i & \mathbf{t}_{1i} & \mathbf{t}_{2i} \end{bmatrix}, \tag{28}$$

where $\mathbf{n}_i$ is the chosen contact normal and $\mathbf{t}_{1i}$ and $\mathbf{t}_{2i}$ span the tangent plane. The orientation of this frame is fixed consistently with the normal and tangential compatibility conventions.

First, consider a rigid-body perturbation in which the fingertip material point remains fixed and the local coordinate frame rotates with the object. Let $\delta\mathbf{u}$ denote object translation and $\delta\boldsymbol{\theta}$ its infinitesimal rotation. Define

$$\mathbf{S} = [\delta\boldsymbol{\theta}]_\times, \qquad \mathbf{Q}(\varepsilon) = \exp(\varepsilon\mathbf{S}), \tag{29}$$

where ε is a scalar perturbation parameter.

For this fixed-material-point model, the relative displacement can be written as

$$\boldsymbol{\phi}_i(\varepsilon) = \mathbf{C}_i^T \mathbf{Q}(\varepsilon)^T \left[\mathbf{r}_i - \varepsilon\delta\mathbf{u} - \mathbf{Q}(\varepsilon)\mathbf{r}_i\right]. \tag{30}$$

Expansion about $\varepsilon = 0$ gives

$$\begin{aligned} \boldsymbol{\phi}_i(\varepsilon) = & -\varepsilon\mathbf{C}_i^T\left(\delta\mathbf{u} + \mathbf{S}\mathbf{r}_i\right) \\ & + \frac{\varepsilon^2}{2}\mathbf{C}_i^T\left(\mathbf{S}^2\mathbf{r}_i + 2\mathbf{S}\delta\mathbf{u}\right) + O(\varepsilon^3). \end{aligned} \tag{31}$$

Thus, the second directional variation associated with this rigid-body mapping is

$$\mathbf{\Gamma}_i^{\text{rigid}} = \mathbf{C}_i^T\left(\mathbf{S}^2\mathbf{r}_i + 2\mathbf{S}\delta\mathbf{u}\right). \tag{32}$$

Its normal and tangential components are

$$\Gamma_{n,i}^{\text{rigid}} = \mathbf{n}_i^T \left(\mathbf{S}^2 \mathbf{r}_i + 2\mathbf{S}\delta\mathbf{u} \right), \tag{33}$$

$$\mathbf{\Gamma}_{t,i}^{\text{rigid}} = \begin{bmatrix} \mathbf{t}_{1i}^T \\ \mathbf{t}_{2i}^T \end{bmatrix} \left(\mathbf{S}^2 \mathbf{r}_i + 2\mathbf{S}\delta\mathbf{u} \right). \tag{34}$$

These expressions show that second-order contributions arise from object rotation and translation–rotation coupling, even when the fingertip material points are fixed.

A distinct geometric effect is associated with local surface curvature. For two externally contacting spheres, the quadratic coefficient of the local normal-separation function is determined by their relative curvature.

If $\delta\mathbf{s}_i$ denotes a small relative tangential displacement in a common tangent plane, the local normal-separation magnitude has the expansion

$$\Delta_{n,i}^{\text{curv}} = \frac{1}{2} \left(\frac{1}{R} + \frac{1}{R_f} \right) \|\delta\mathbf{s}_i\|^2 + O(\|\delta\mathbf{s}_i\|^4). \tag{35}$$

The corresponding quadratic coefficient is

$$\Gamma_{n,i}^{\text{curv}} = \left(\frac{1}{R} + \frac{1}{R_f} \right) \|\delta\mathbf{s}_i\|^2. \tag{36}$$

The sign of this contribution in the normal compatibility equation depends on the adopted normal-gap convention.

The rigid-body expressions (33)–(34) and the curvature expression (36) describe different kinematic constructions. They must not be added independently without establishing a common nonlinear contact mapping, since the resulting model could otherwise omit or double-count geometric effects.

For numerical implementation, the normal and tangential corrections must therefore be evaluated from the particular contact mapping adopted for the example, with consistent perturbation variables and Jacobian derivatives.

The resulting second-order compatibility relations are incorporated into the MNCP formulation developed in Section 4.

4 Complementarity Formulation

The contact problem is formulated by combining second-order contact kinematics with unilateral contact conditions and nonlinear friction laws. The resulting system belongs to the class of mixed complementarity problems (MCPs), which extend nonlinear complementarity problems by incorporating equality constraints [30, 12]. Since the governing contact and friction relations are nonlinear, the formulation is referred to here as a mixed nonlinear complementarity problem (MNCP).

4.1 Contact Force Representation

The contact force vector is written as

$$\mathbf{f} = \begin{bmatrix} \mathbf{f}_n \\ \mathbf{f}_t \end{bmatrix}, \tag{37}$$

where $\mathbf{f}_n \in \mathbb{R}^n$ is the vector of normal forces and $\mathbf{f}_t \in \mathbb{R}^{2n}$ is the tangential force vector.

To enforce nonnegativity, the tangential force is decomposed as

$$\mathbf{f}_t = \mathbf{f}_t^+ - \mathbf{f}_t^-, \qquad \mathbf{f}_t^+ \geq 0, \quad \mathbf{f}_t^- \geq 0. \tag{38}$$

4.2 Unilateral Contact Conditions

The normal contact conditions are expressed as

$$\mathbf{y}_n \geq 0, \quad \mathbf{f}_n \geq 0, \quad \mathbf{y}_n^T \mathbf{f}_n = 0. \tag{39}$$

The tangential displacement is decomposed consistently as

$$\mathbf{y}_t = \mathbf{y}_t^+ - \mathbf{y}_t^-, \qquad \mathbf{y}_t^+ \geq 0, \quad \mathbf{y}_t^- \geq 0. \tag{40}$$

Similarly, the tangential complementarity conditions are written as

$$\mathbf{y}_t^+ \geq 0, \quad \mathbf{f}_t^+ \geq 0, \quad (\mathbf{y}_t^+)^T \mathbf{f}_t^+ = 0, \tag{41}$$
$$\mathbf{y}_t^- \geq 0, \quad \mathbf{f}_t^- \geq 0, \quad (\mathbf{y}_t^-)^T \mathbf{f}_t^- = 0. \tag{42}$$

Taking into account the relation given in (38), the friction law given by (17) can be written in compact form as [17]

$$\psi_i = B_{ni}(f_{ni}) f_{ni} - \mathbf{B}_{tti} \mathbf{f}_{ti}^+ + \mathbf{B}_{tti} \mathbf{f}_{ti}^-, \quad i = 1, 2, \ldots, n, \tag{43}$$

where

$$\begin{aligned}
B_{ni}(f_{ni}) &= f_{ni}, \\
\mathbf{B}_{tti} &= \mathbf{B}_{ti1}(\mathbf{f}_{ti}^+) - \mathbf{B}_{ti2}(\mathbf{f}_{ti}^-) \\
\mathbf{B}_{ti1}(\mathbf{f}_{ti}^+) &= \begin{bmatrix} \dfrac{f_{ti1}^+}{\mu_{i1}^2} & \dfrac{f_{ti2}^+}{\mu_{i2}^2} \end{bmatrix}, \\
\mathbf{B}_{ti2}(\mathbf{f}_{ti}^-) &= \begin{bmatrix} \dfrac{f_{ti1}^-}{\mu_{i1}^2} & \dfrac{f_{ti2}^-}{\mu_{i2}^2} \end{bmatrix}, \\
\mathbf{f}_{ti}^+ &= \begin{bmatrix} f_{ti1}^+ & f_{ti2}^+ \end{bmatrix}^T, \\
\mathbf{f}_{ti}^- &= \begin{bmatrix} f_{ti1}^- & f_{ti2}^- \end{bmatrix}^T.
\end{aligned}$$

For the whole gripper–object system, the friction law can be written as

$$\boldsymbol{\psi} = \mathbf{B}_n(\mathbf{f}_n)\mathbf{f}_n - \mathbf{B}_{tt}\mathbf{f}_t^+ + \mathbf{B}_{tt}\mathbf{f}_t^-, \tag{44}$$

where

$$\begin{aligned}
\mathbf{B}_n &= \mathrm{diag}[B_{n1}, B_{n2}, \ldots, B_{nn}], \\
\mathbf{B}_{tt} &= \mathrm{diag}[\mathbf{B}_{tt1}, \mathbf{B}_{tt2}, \ldots, \mathbf{B}_{ttn}], \\
\mathbf{f}_t^+ &= [\mathbf{f}_{t1}^+, \mathbf{f}_{t2}^+, \ldots, \mathbf{f}_{tn}^+]^T, \\
\mathbf{f}_t^- &= [\mathbf{f}_{t1}^-, \mathbf{f}_{t2}^-, \ldots, \mathbf{f}_{tn}^-]^T.
\end{aligned}$$

Taking into account (43), the nonnegative slipping vectors in (19) can be written as

$$\mathbf{y}_t^+ = \mathbf{B}_{t2}^T(\mathbf{f}_t^-)\boldsymbol{\lambda}, \qquad \mathbf{y}_t^- = \mathbf{B}_{t1}^T(\mathbf{f}_t^+)\boldsymbol{\lambda}, \qquad \boldsymbol{\lambda} \geq \mathbf{0}. \tag{45}$$

Here

$$\begin{aligned}
\mathbf{B}_{t1} &= \mathrm{diag}[\mathbf{B}_{t11}, \mathbf{B}_{t21}, \ldots, \mathbf{B}_{tn1}], \\
\mathbf{B}_{t2} &= \mathrm{diag}[\mathbf{B}_{t12}, \mathbf{B}_{t22}, \ldots, \mathbf{B}_{tn2}],
\end{aligned}$$

The operators $\mathbf{B}_{t1}$ and $\mathbf{B}_{t2}$ define the slipping direction opposite to the corresponding tangential force components, ensuring consistency with the Coulomb friction law. The vectors $\boldsymbol{\psi}$ and the nonnegative slipping parameters $\boldsymbol{\lambda}$ fulfill the orthogonality condition

$$\boldsymbol{\psi}^T \boldsymbol{\lambda} = 0. \tag{46}$$

Since the direction of slipping is opposite to the friction forces, the following orthogonality conditions are obtained:

$$(\mathbf{y}_t^+)^T \mathbf{f}_t^+ = 0, \qquad (\mathbf{y}_t^-)^T \mathbf{f}_t^- = 0. \tag{47}$$

4.3 Contact Compatibility Relations

Let the rigid-body displacements be expressed as a difference of two nonnegative vectors:

$$\mathbf{u}_o = \mathbf{u}_o^+ - \mathbf{u}_o^-. \tag{48}$$

From the second-order kinematic formulation, and taking into account (6), (8), (16), (38)–(42), (47), and (48), the relative displacements at the contacts expressed in (26) and (27) become

$$\begin{aligned} \mathbf{y}_n &= \mathbf{F}_{11}\mathbf{f}_n + \mathbf{F}_{12}\mathbf{f}_t^+ - \mathbf{F}_{12}\mathbf{f}_t^- + \mathbf{G}_n^T\mathbf{u}_o^+ - \mathbf{G}_n^T\mathbf{u}_o^- \\ &\quad + \frac{1}{2}\boldsymbol{\Gamma}_n(\delta\boldsymbol{\eta}, \delta\boldsymbol{\eta}) + \mathbf{c}_n, \end{aligned} \tag{49}$$

$$\begin{aligned} \mathbf{y}_t^+ &= \mathbf{F}_{21}\mathbf{f}_n + \mathbf{F}_{22}\mathbf{f}_t^+ - \mathbf{F}_{22}\mathbf{f}_t^- + \mathbf{G}_t^T\mathbf{u}_o^+ - \mathbf{G}_t^T\mathbf{u}_o^- \\ &\quad + \frac{1}{2}\boldsymbol{\Gamma}_t(\delta\boldsymbol{\eta}, \delta\boldsymbol{\eta}) + \mathbf{B}_{t1}^T(\mathbf{f}_t^+)\boldsymbol{\lambda} + \mathbf{c}_t, \end{aligned} \tag{50}$$

$$\begin{aligned} \mathbf{y}_t^- &= -\mathbf{F}_{21}\mathbf{f}_n - \mathbf{F}_{22}\mathbf{f}_t^+ + \mathbf{F}_{22}\mathbf{f}_t^- - \mathbf{G}_t^T\mathbf{u}_o^+ + \mathbf{G}_t^T\mathbf{u}_o^- \\ &\quad - \frac{1}{2}\boldsymbol{\Gamma}_t(\delta\boldsymbol{\eta}, \delta\boldsymbol{\eta}) + \mathbf{B}_{t2}^T(\mathbf{f}_t^-)\boldsymbol{\lambda} - \mathbf{c}_t. \end{aligned} \tag{51}$$

where the rigid-body displacement $\mathbf{u}_o$ and the joint variation $\delta\mathbf{q}$ are kept explicit, while the quadratic term depends on the infinitesimal perturbation vector $\delta\boldsymbol{\eta}$.

Here

$$\mathbf{F} = \begin{bmatrix} \mathbf{F}_{11} & \mathbf{F}_{12} & -\mathbf{F}_{12} \\ \mathbf{F}_{21} & \mathbf{F}_{22} & -\mathbf{F}_{22} \\ -\mathbf{F}_{21} & -\mathbf{F}_{22} & \mathbf{F}_{22} \end{bmatrix}, \tag{52}$$

where

$$\begin{aligned} \mathbf{F}_{11} &= \mathbf{F}_{nn} + \mathbf{J}_n\mathbf{F}_j\mathbf{J}_n^T, \qquad \mathbf{F}_{12} = \mathbf{F}_{nt} + \mathbf{J}_n\mathbf{F}_j\mathbf{J}_t^T, \\ \mathbf{F}_{21} &= \mathbf{F}_{tn} + \mathbf{J}_t\mathbf{F}_j\mathbf{J}_n^T, \qquad \mathbf{F}_{22} = \mathbf{F}_{tt} + \mathbf{J}_t\mathbf{F}_j\mathbf{J}_t^T. \end{aligned}$$

Taking into account (38) and introducing the nonnegative slack variables $\mathbf{v}^+ \geq \mathbf{0}$ and $\mathbf{v}^- \geq \mathbf{0}$ in (1), one obtains

$$\mathbf{v}^+ = -\mathbf{G}_n\mathbf{f}_n - \mathbf{G}_t\mathbf{f}_t^+ + \mathbf{G}_t\mathbf{f}_t^- + \mathbf{P}, \tag{53}$$

$$\mathbf{v}^- = \mathbf{G}_n\mathbf{f}_n + \mathbf{G}_t\mathbf{f}_t^+ - \mathbf{G}_t\mathbf{f}_t^- - \mathbf{P}. \tag{54}$$

The complementary energy is defined as

$$\Pi(\mathbf{f}) = \frac{1}{2}\mathbf{f}^T\mathbf{F}\mathbf{f} + \mathbf{c}^T\mathbf{f}. \tag{55}$$

The second-order optimal grasping problem is thus formulated as

$$\min_{\mathbf{f}, \delta\mathbf{q}, \boldsymbol{\lambda}} \ \Pi(\mathbf{f}) \tag{56}$$

subject to

$$
\begin{aligned}
\mathbf{y}_n &= \mathbf{F}_{11}\mathbf{f}_n + \mathbf{F}_{12}\mathbf{f}_t^+ - \mathbf{F}_{12}\mathbf{f}_t^- + \mathbf{G}_n^T\mathbf{u}_o^+ - \mathbf{G}_n^T\mathbf{u}_o^- \\
&\quad + \frac{1}{2}\boldsymbol{\Gamma}_n(\delta\boldsymbol{\eta},\delta\boldsymbol{\eta}) + \mathbf{c}_n, \\
\mathbf{y}_t^+ &= \mathbf{F}_{21}\mathbf{f}_n + \mathbf{F}_{22}\mathbf{f}_t^+ - \mathbf{F}_{22}\mathbf{f}_t^- + \mathbf{G}_t^T\mathbf{u}_o^+ - \mathbf{G}_t^T\mathbf{u}_o^- \\
&\quad + \frac{1}{2}\boldsymbol{\Gamma}_t(\delta\boldsymbol{\eta},\delta\boldsymbol{\eta}) + \mathbf{B}_{t1}^T(\mathbf{f}_t^+)\boldsymbol{\lambda} + \mathbf{c}_t, \\
\mathbf{y}_t^- &= -\mathbf{F}_{21}\mathbf{f}_n - \mathbf{F}_{22}\mathbf{f}_t^+ + \mathbf{F}_{22}\mathbf{f}_t^- - \mathbf{G}_t^T\mathbf{u}_o^+ + \mathbf{G}_t^T\mathbf{u}_o^- \\
&\quad - \frac{1}{2}\boldsymbol{\Gamma}_t(\delta\boldsymbol{\eta},\delta\boldsymbol{\eta}) + \mathbf{B}_{t2}^T(\mathbf{f}_t^-)\boldsymbol{\lambda} - \mathbf{c}_t, \\
\mathbf{v}^+ &= -\mathbf{G}_n\mathbf{f}_n - \mathbf{G}_t\mathbf{f}_t^+ + \mathbf{G}_t\mathbf{f}_t^- + \mathbf{P}, \\
\mathbf{v}^- &= \mathbf{G}_n\mathbf{f}_n + \mathbf{G}_t\mathbf{f}_t^+ - \mathbf{G}_t\mathbf{f}_t^- - \mathbf{P}, \\
\boldsymbol{\psi} &= \mathbf{B}_n(\mathbf{f}_n)\mathbf{f}_n - \mathbf{B}_{tt}\mathbf{f}_t^+ + \mathbf{B}_{tt}\mathbf{f}_t^-,
\end{aligned}
$$

and

$$
\begin{aligned}
&\mathbf{0} \le \mathbf{y}_n \perp \mathbf{f}_n \ge \mathbf{0}, \\
&\mathbf{0} \le \mathbf{y}_t^+ \perp \mathbf{f}_t^+ \ge \mathbf{0}, \qquad \mathbf{0} \le \mathbf{y}_t^- \perp \mathbf{f}_t^- \ge \mathbf{0}, \\
&\mathbf{0} \le \mathbf{v}^+ \perp \mathbf{u}_o^+ \ge \mathbf{0}, \qquad \mathbf{0} \le \mathbf{v}^- \perp \mathbf{u}_o^- \ge \mathbf{0}, \\
&\mathbf{0} \le \boldsymbol{\psi} \perp \boldsymbol{\lambda} \ge \mathbf{0}.
\end{aligned} \tag{57}
$$

The slack variables $\mathbf{v}^+ \ge \mathbf{0}$ and $\mathbf{v}^- \ge \mathbf{0}$ must vanish at the equilibrium point, and thus the following orthogonality holds:

$$
(\mathbf{v}^+)^T\mathbf{u}_o^+ = 0, \qquad (\mathbf{v}^-)^T\mathbf{u}_o^- = 0. \tag{58}
$$

The resulting MNCP therefore combines equilibrium, contact compatibility, unilateral contact, nonlinear friction, and the second-order geometric corrections within a single complementarity framework.

5 Solution Methods and Analysis

5.1 Solution Methods

The mixed nonlinear complementarity problem (MNCP) derived in Section 4 provides a complete description of the second-order grasping problem. This system is solved directly using complementarity-based numerical methods. In addition, the complementary energy formulation offers an optimization-based interpretation of the grasping problem and its contact-force distribution.

The complementary energy of the grasping system is defined as

$$
\Pi(\bar{\mathbf{f}}) = \frac{1}{2}\bar{\mathbf{f}}^T\mathbf{F}\bar{\mathbf{f}} + \mathbf{c}^T\bar{\mathbf{f}}, \tag{59}
$$

where $\bar{\mathbf{f}} = [\mathbf{f}_n^T \ (\mathbf{f}_t^+)^T \ (\mathbf{f}_t^-)^T]^T$ denotes the vector of nonnegative contact force components, partitioned according to the decomposition $\mathbf{f}_t = \mathbf{f}_t^+ - \mathbf{f}_t^-$ introduced in (38).

5.1.1 Mathematical Program with Complementarity Constraints

An associated mathematical program with complementarity constraints (MPCC) can be formulated by minimizing the complementary-energy function over the feasible set defined by the MNCP conditions:

$$
\min_{\bar{\mathbf{f}},\mathbf{u}_o^+,\mathbf{u}_o^-,\boldsymbol{\lambda}} \ \Pi(\bar{\mathbf{f}}) \tag{60}
$$

subject to the nonlinear kinematic constraints (49)–(51), the equilibrium relations (53)– (54), the friction law (44), and the complementarity conditions (57). The auxiliary variables $\mathbf{u}_o^+$, $\mathbf{u}_o^-$, and $\boldsymbol{\lambda}$ are determined implicitly by these constraints; they are listed as optimization variables for completeness of the formulation.

The present numerical approach solves the MNCP feasibility conditions directly rather than minimizing the complementary-energy objective. Accordingly, no general equivalence between MNCP feasibility and complementary-energy minimization is assumed.

Because the complementarity constraints make the feasible set nonconvex and nonsmooth, the MPCC is not solved directly as an optimization problem. Instead, the complementarity conditions are reformulated using the Fischer–Burmeister function, as described below, and the resulting nonlinear system is solved using a semismooth Newton method.

5.1.2 Fischer–Burmeister Reformulation and Semismooth Newton Method

The MNCP is solved by reformulating its complementarity conditions as a system of nonlinear equations using the Fischer–Burmeister (FB) function [25, 26, 27]. For two scalars a and b, the exact FB function is defined as

$$\phi_{\mathrm{FB}}(a,b) = \sqrt{a^2+b^2} - (a+b). \tag{61}$$

It satisfies

$$\phi_{\mathrm{FB}}(a,b) = 0 \quad \Longleftrightarrow \quad a \geq 0, \quad b \geq 0, \quad ab = 0. \tag{62}$$

Hence, each complementarity pair in the MNCP can be replaced by an equivalent FB equation.

In practice, a regularized form is used,

$$\phi^{\varepsilon}_{\mathrm{FB}}(a,b) = \sqrt{a^2+b^2+\varepsilon^2} - (a+b), \tag{63}$$

where $\varepsilon > 0$ is a small regularization parameter that ensures differentiability at the origin. The regularized and exact forms coincide as $\varepsilon \to 0$; in the numerical examples reported below, $\varepsilon = 10^{-9}$ is used.

Let the vector of unknowns be denoted by

$$\mathbf{z} = \begin{bmatrix} \mathbf{f}_n^T & (\mathbf{f}_t^+)^T & (\mathbf{f}_t^-)^T & (\mathbf{u}_o^+)^T & (\mathbf{u}_o^-)^T & \boldsymbol{\lambda}^T \end{bmatrix}^T. \tag{64}$$

For vectors $\mathbf{a}$ and $\mathbf{b}$ of equal dimension, define the FB operator componentwise by

$$\boldsymbol{\phi}_{\mathrm{FB}}(\mathbf{a},\mathbf{b}) = \begin{bmatrix} \phi_{\mathrm{FB}}(a_1,b_1) \\ \vdots \\ \phi_{\mathrm{FB}}(a_m,b_m) \end{bmatrix}. \tag{65}$$

Using the complementarity pairs of the MNCP, the nonlinear residual mapping is assembled as

$$\boldsymbol{\Phi}(\mathbf{z}) = \begin{bmatrix} \boldsymbol{\phi}_{\mathrm{FB}}(\mathbf{y}_n, \mathbf{f}_n) \\ \boldsymbol{\phi}_{\mathrm{FB}}(\mathbf{y}_t^+, \mathbf{f}_t^+) \\ \boldsymbol{\phi}_{\mathrm{FB}}(\mathbf{y}_t^-, \mathbf{f}_t^-) \\ \boldsymbol{\phi}_{\mathrm{FB}}(\mathbf{v}^+, \mathbf{u}_o^+) \\ \boldsymbol{\phi}_{\mathrm{FB}}(\mathbf{v}^-, \mathbf{u}_o^-) \\ \boldsymbol{\phi}_{\mathrm{FB}}(\boldsymbol{\psi}, \boldsymbol{\lambda}) \end{bmatrix}. \tag{66}$$

The MNCP is therefore equivalently represented by

$$\boldsymbol{\Phi}(\mathbf{z}) = \mathbf{0}. \tag{67}$$

Because the Fischer–Burmeister function is semismooth, the resulting system is solved by a semismooth Newton method. At iteration k, a generalized Newton direction $\Delta\mathbf{z}^k$ is obtained from

$$\mathbf{J}_k \Delta\mathbf{z}^k = -\boldsymbol{\Phi}(\mathbf{z}^k), \qquad \mathbf{J}_k \in \partial\boldsymbol{\Phi}(\mathbf{z}^k), \tag{68}$$

where $\partial\boldsymbol{\Phi}$ denotes the Clarke generalized Jacobian of the FB mapping. For the regularized FB function (63), the generalized Jacobian is single-valued and equals the ordinary Jacobian,

$$\frac{\partial \phi^{\varepsilon}_{\mathrm{FB}}}{\partial a} = \frac{a}{\sqrt{a^2+b^2+\varepsilon^2}} - 1, \qquad \frac{\partial \phi^{\varepsilon}_{\mathrm{FB}}}{\partial b} = \frac{b}{\sqrt{a^2+b^2+\varepsilon^2}} - 1. \tag{69}$$

The iterate is updated as

$$\mathbf{z}^{k+1} = \mathbf{z}^k + \alpha_k \Delta\mathbf{z}^k, \tag{70}$$

where $\alpha_k \in (0,1]$ is determined by a backtracking line search that enforces the Armijo sufficient-decrease condition for the merit function

$$m(\mathbf{z}) = \frac{1}{2}\|\mathbf{\Phi}(\mathbf{z})\|_2^2. \tag{71}$$

Starting from $\alpha = 1$, the step is halved until

$$m(\mathbf{z}^k + \alpha\Delta\mathbf{z}^k) \le m(\mathbf{z}^k) + c\,\alpha\,\nabla m(\mathbf{z}^k)^T\Delta\mathbf{z}^k, \tag{72}$$

where $c \in (0,1)$ is a small constant (e.g., $c = 10^{-4}$).

Convergence is declared when

$$\|\mathbf{\Phi}(\mathbf{z}^k)\|_2 \le \varepsilon_{\text{tol}}, \tag{73}$$

for a prescribed tolerance ε_{tol} (e.g., $\varepsilon_{\text{tol}} = 10^{-8}$). If the step size or the residual stagnates before reaching this tolerance, the iteration is terminated and the result is reported as non-converged.

5.1.3 Numerical Remarks

The resulting grasp problem is nonlinear and nonsmooth because of the frictional contact laws and the complementarity conditions. These features are present independently of the second-order kinematic correction. The term $\mathbf{\Gamma}(\delta\boldsymbol{\eta}, \delta\boldsymbol{\eta})$ introduces an additional quadratic dependence on the perturbation variables and therefore increases the nonlinearity of the contact kinematic mapping. It should not, however, be regarded as the sole source of nonconvexity of the frictional contact problem.

From a numerical standpoint, the nonconvexity of the MNCP implies that the semismooth Newton method is only locally convergent: different initial guesses may lead to different solutions, and some initial guesses may not converge at all. This behavior is inherent to the complementarity formulation and is not specific to the second-order correction. In the numerical examples reported below, the solver is initialized from a physically motivated preload, and the convergence behavior is documented in terms of iteration count and final residual.

5.2 Equilibrium Feasibility under Perturbations

The second-order formulation provides a natural framework for examining whether contact equilibrium remains feasible under small but finite perturbations of the reference grasp configuration. This analysis should be distinguished from a general dynamical or Lyapunov definition of grasp stability.

Formally, let $\delta\boldsymbol{\eta}$ be a prescribed admissible perturbation of the reference configuration. The perturbed grasp is *equilibrium-feasible* if there exist contact forces $\mathbf{f}$ and auxiliary variables $(\mathbf{u}_o^{\pm}, \boldsymbol{\lambda})$ satisfying the MNCP of Section 4 at the perturbed configuration.

The second-order correction $\mathbf{\Gamma}(\delta\boldsymbol{\eta}, \delta\boldsymbol{\eta})$ modifies the contact compatibility relations and therefore may alter the set of perturbations for which such an admissible equilibrium exists. Comparing the first- and second-order formulations for a given perturbation therefore provides a measure of the influence of local contact geometry on equilibrium feasibility.

This analysis does not constitute a general dynamic stability criterion. Rather, it evaluates the persistence of admissible quasi-static equilibrium under local perturbations. The numerical examples in Section 6 illustrate this comparison for representative perturbations.

5.3 Existence and Numerical Remarks

The formulation developed above defines a nonlinear complementarity system involving equilibrium, second-order contact kinematics, unilateral contact, and nonlinear friction constraints. Existence and uniqueness of a solution are not guaranteed solely by the positive definiteness of the compliance matrix.

For first-order complementarity formulations, existence results are available under appropriate assumptions on the complementarity mapping and the feasible set [12]. However, such assumptions, including the required monotonicity or other sufficient existence conditions, are not established here for the general frictional grasping problem. The second-order geometric correction introduces additional nonlinear dependence on the perturbation variables, and the resulting MNCP does not necessarily satisfy these conditions.

Depending on the contact geometry, friction parameters, loading conditions, and reference configuration, the resulting MNCP may admit more than one admissible solution. Accordingly, the numerical solution

obtained by the semismooth Newton method is verified a posteriori by evaluating the final complementarity residual together with the equilibrium, unilateral-contact, and friction conditions. The numerical examples in Section 6 report these quantities together with the convergence behavior of the solver.

6 Numerical Examples

This section presents three numerical examples with complementary objectives. The first considers a planar two-finger grasp and is used to illustrate directly the curvature-induced quadratic correction to the contact gap. The second considers a free three-dimensional three-finger grasp of a spherical object and demonstrates the proposed MNCP formulation for a general spatial multifingered grasp, with particular emphasis on the contact-force distribution and frictional admissibility. The third considers a sphere supported by a horizontal table and subjected to an external torque about the vertical axis; this configuration provides an independently solvable benchmark for validating the force equilibrium, moment equilibrium, friction, and complementarity implementation.

The fingers are represented at the contact level through their contact locations, local contact frames, friction properties, and effective compliance. An explicit multi-joint hand model is not introduced, since the objective is to isolate the effects of local contact geometry and second-order kinematics from those associated with a particular robotic hand architecture. Because the formulation is developed at the contact level, the numerical results are independent of any particular kinematic architecture.

The resulting nonlinear complementarity systems are reformulated using the Fischer–Burmeister (FB) function and solved using a regularized semismooth Newton method. The mechanical equilibrium residual and the FB residual are used to verify the numerical solutions, while the contact-force distribution and friction margin are used to assess the physical influence of the second-order terms.

To facilitate reproducibility, the numerical examples are presented with the relevant contact geometry, compliance parameters, initial contact offsets, and prescribed perturbations. The local contact frames, grasp matrices, and second-order geometric corrections are constructed following the procedures described in the preceding sections. The MATLAB implementation used to obtain the numerical results and figures is available from the author upon reasonable request.

The principal numerical inputs for the three examples are summarized in Table 1. Additional example-specific parameters and geometric constructions are described in the corresponding subsections.

Table 1: Numerical input data for the three examples.

Parameter	Example 1	Example 2	Example 3
Number of contacts	2	3	3
Object radius (m)	0.050	0.035	0.050
Fingertip radius (m)	0.010	0.012	0.012
Friction coefficients	$\mu = 0.50$	$\mu_1 = \mu_2 = 0.70$	$\mu_1 = 0.50,\ \mu_2 = 0.40$
Normal compliance $\mathbf{F}_{11}$	$10^{-4}\mathbf{I}_2$	$\mathbf{I}_3$	$0.1\mathbf{I}_3$
Tangential compliance $\mathbf{F}_{22}$	$10^{-4}\mathbf{I}_2$	$0.1\mathbf{I}_6$	$0.1\mathbf{I}_6$
Coupling $\mathbf{F}_{12}$	$\mathbf{0}_{2\times 2}$	$0.05\mathbf{1}_{3\times 6}$	$\mathbf{0}_{3\times 6}$
Coupling $\mathbf{F}_{21}$	$\mathbf{F}_{12}^T$	$\mathbf{F}_{12}^T$	$\mathbf{F}_{12}^T$
Normal offsets $\mathbf{c}_n$	$\mathbf{0}_2$	$\mathbf{0}_3$	$-\mathbf{1}_3$
Tangential offsets $\mathbf{c}_t$	$\mathbf{0}_2$	$\mathbf{0}_6$	See text
Curvature perturbation	$s \in [-5, 5]$ mm	$\delta = 2$ mm	$\delta = 2$ mm
Rigid-frame translation (m)	Not applied	$[0.001, 0, 0]^T$	$[0.001, 0, 0]^T$
Rigid-frame rotation (rad)	Not applied	$[0.01, 0.02, 0.01]^T$	$[0.01, 0.02, 0.01]^T$

For Example 3, the initial tangential offsets are computed from the analytical reference contact forces as $\mathbf{c}_t = -\mathbf{F}_{22}\mathbf{f}_t^{\mathrm{ref}}$. The contact locations, local frames, grasp matrices, and geometric corrections are constructed as described in the corresponding numerical examples.

6.1 Planar Two-Finger Grasp

A planar two-finger grasp of a circular object is first considered to illustrate the geometric effect of the second-order contact model. The object radius is $R_o = 0.05$ m, and the fingertip radius is $R_f = 0.01$ m. The corresponding relative curvature is

$$\kappa = \frac{1}{R_o} + \frac{1}{R_f} = 120 \text{ m}^{-1}.$$

The friction coefficient is $\mu = 0.5$, and the effective compliance is taken as $\mathbf{F} = 10^{-4}\mathbf{I}$. The grasp geometry is shown in Figure 2. The two contacts are located on opposite sides of the circular object, with local normal and tangential directions defined at each contact.

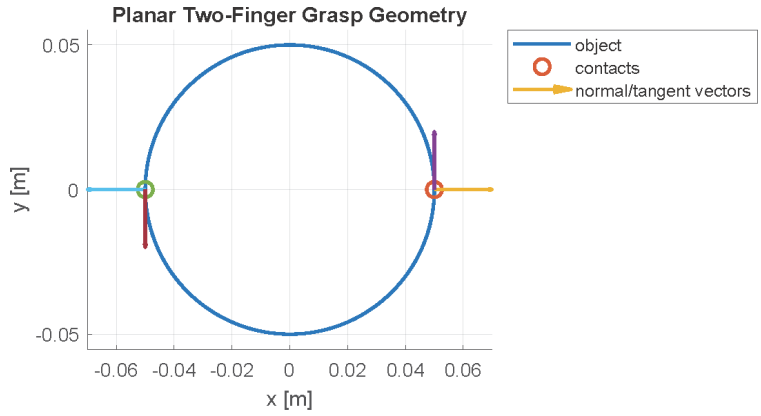


Figure 2: Planar two-finger grasp used to illustrate second-order contact geometry.

For infinitesimal relative motion, the conventional first-order model retains only the linear variation of the contact gap. For curved contacting surfaces, however, tangential relative motion also produces a second-order variation in the normal gap. In the proposed formulation, this contribution is represented by $\frac{1}{2}\boldsymbol{\Gamma}_n(\delta\boldsymbol{\eta}, \delta\boldsymbol{\eta})$. Figure 3 compares the first-order and second-order normal-gap predictions. The two models approach one another for small perturbations, whereas the curvature-dependent quadratic contribution becomes increasingly apparent as the tangential perturbation increases. The example therefore provides a direct geometric illustration of the information neglected when the contact kinematics are truncated at first order.

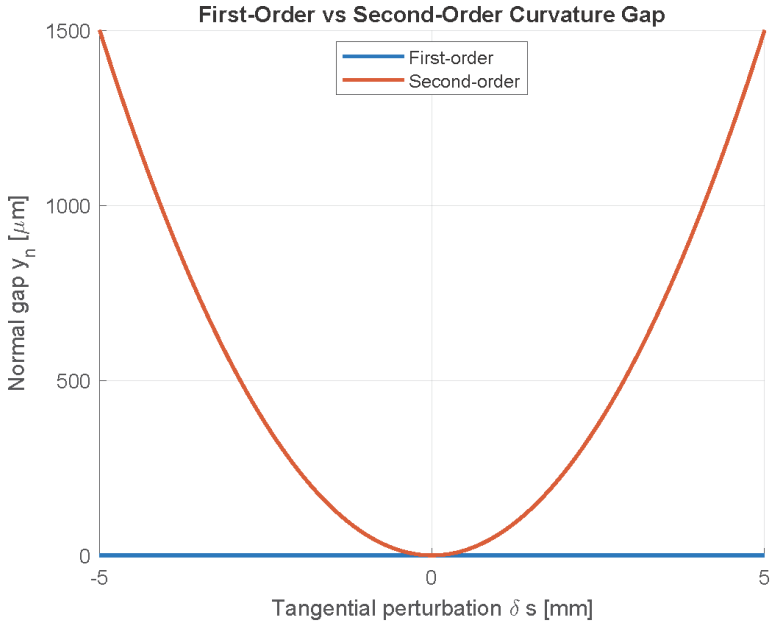


Figure 3: Comparison of first-order and second-order normal-gap predictions.

6.2 Free Spatial Three-Finger Grasp of a Spherical Object

A free spatial grasp of a spherical object by three hard-finger contacts is considered to assess the proposed mixed nonlinear complementarity problem (MNCP) formulation in three dimensions. Unlike the preceding planar example, the object has no external support, and the applied spatial wrench must be balanced by the finger contacts. The gravity-only case is used to compare four contact-kinematic approximations, while additional moment-loading cases are retained as tests of the first-order and curvature-corrected formulations.

The object has radius $R = 35\,\text{mm}$ and mass $m = 0.15\,\text{kg}$. The contacts are located at polar and azimuthal angles

$$(\theta_i, \phi_i) = (125^\circ, 0^\circ), \quad (110^\circ, 130^\circ), \quad (115^\circ, 240^\circ),$$

where θ_i is measured from the positive z-axis. An inward normal and two orthogonal tangent directions define each local contact frame. The resulting spatial grasp matrix has rank six and condition number 47.55. Figure 4 shows the contact arrangement.

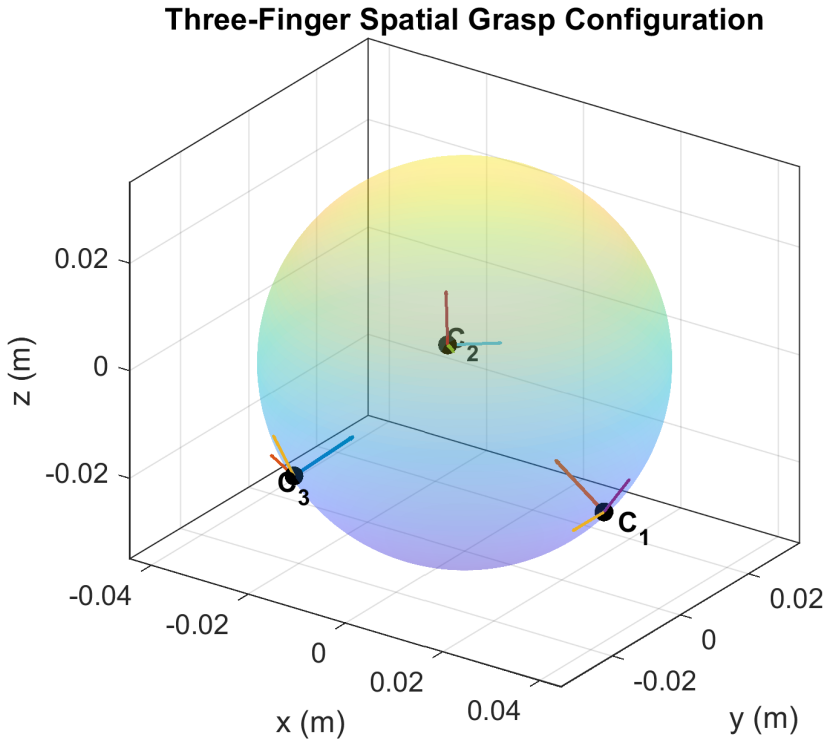


Figure 4: Three-finger spatial grasp and local contact frames.

The friction coefficients are $\mu_{1,i} = \mu_{2,i} = 0.70$ for $i = 1, 2, 3$. The formulation also permits different friction coefficients in the two local tangential directions. Gravity produces $\mathbf{F}_g = [0\ 0\ -1.4715]^T\,\text{N}$; with the adopted sign convention, the required balancing contact wrench is

$$\mathbf{P}_0 = [0\ 0\ 1.4715\ 0\ 0\ 0]^T.$$

Additional required wrenches are obtained by adding, separately, a $0.010\,\text{N m}$ moment about each coordinate axis:

$$\mathbf{P}_x = [0\ 0\ 1.4715\ 0.010\ 0\ 0]^T,$$
$$\mathbf{P}_y = [0\ 0\ 1.4715\ 0\ 0.010\ 0]^T,$$
$$\mathbf{P}_z = [0\ 0\ 1.4715\ 0\ 0\ 0.010]^T.$$

6.2.1 Second-order contact geometry and model definitions

Each fingertip is locally approximated by a sphere of radius $R_f = 12\,\text{mm}$. The relative normal curvature is

$$\kappa = \frac{1}{R} + \frac{1}{R_f} = 111.9048\,\text{m}^{-1}.$$

The analytical normal-contact Hessian $\mathbf{H}_i$ has one zero normal eigenvalue and two equal tangential eigenvalues:

$$\mathrm{eig}(\mathbf{H}_i) \simeq \{0, 111.9048, 111.9048\}\,\mathrm{m}^{-1}.$$

These values agree with the numerically evaluated Hessians to numerical precision. The prescribed tangential perturbation at contact i is

$$\delta\mathbf{x}_i = \delta\mathbf{t}_{1,i} + \delta\mathbf{t}_{2,i}, \qquad \delta = 2\times10^{-3}\,\mathrm{m}, \tag{74}$$

where $\mathbf{t}_{1,i}$ and $\mathbf{t}_{2,i}$ are the unit tangent vectors of the local contact frame. A prescribed 2 mm displacement in each of the two local tangent directions yields

$$\Gamma_{n,i}^{\mathrm{curv}} = \delta\mathbf{x}_i^T\mathbf{H}_i\delta\mathbf{x}_i \simeq 4.47619\times10^{-4}\,\mathrm{m}, \qquad i = 1,2,3.$$

The corresponding Taylor contribution to normal compatibility is $\frac{1}{2}\Gamma_{n,i}^{\mathrm{curv}}$.

Four models are compared under gravity-only loading:

- **M1 (first order):** $\boldsymbol{\Gamma}_n = \mathbf{0}$ and $\boldsymbol{\Gamma}_t = \mathbf{0}$.
- **M2 (normal curvature):** $\boldsymbol{\Gamma}_n = \boldsymbol{\Gamma}_n^{\mathrm{curv}}$ and $\boldsymbol{\Gamma}_t = \mathbf{0}$.
- **M3 (normal curvature and rigid-frame tangential correction):** $\boldsymbol{\Gamma}_n = \boldsymbol{\Gamma}_n^{\mathrm{curv}}$ and $\boldsymbol{\Gamma}_t = \boldsymbol{\Gamma}_t^{\mathrm{rigid}}$.
- **M4 (composite correction):** $\boldsymbol{\Gamma}_n = \boldsymbol{\Gamma}_n^{\mathrm{curv}} + \boldsymbol{\Gamma}_n^{\mathrm{rigid}}$ and $\boldsymbol{\Gamma}_t = \boldsymbol{\Gamma}_t^{\mathrm{rigid}}$.

The prescribed rigid-frame perturbation consists of the translational increment

$$\delta\mathbf{u} = \begin{bmatrix}10^{-3} & 0 & 0\end{bmatrix}^T\,\mathrm{m} \tag{75}$$

and the rotational increment

$$\delta\boldsymbol{\theta} = \begin{bmatrix}0.01 & 0.02 & 0.01\end{bmatrix}^T\,\mathrm{rad}. \tag{76}$$

The prescribed rigid-frame corrections are obtained from the second directional variation of a rigid-frame contact mapping, using the same perturbation for the normal and tangential components. For this test,

$$\boldsymbol{\Gamma}_n^{\mathrm{rigid}} \simeq 10^{-6}[-2.1541\ -7.9306\ -1.1394]^T\,\mathrm{m},$$

$$\boldsymbol{\Gamma}_t^{\mathrm{rigid}} \simeq 10^{-4}[-0.2172\ -0.3157\ 0.1640\ -0.3020\ 0.0885\ -0.4326]^T\,\mathrm{m}.$$

The correction vectors are prescribed inputs rather than additional MNCP unknowns. M4 is a composite kinematic sensitivity approximation: its normal terms arise from two distinct mappings, so it is not asserted to be the Hessian correction of a single exact sphere–sphere rolling/sliding law.

6.2.2 Numerical solutions and comparison

All models are formulated as MNCPs and solved with the Fischer–Burmeister semismooth Newton method. The system has 30 unknowns, including normal forces, split tangential forces, split kinematic variables, and friction multipliers. The analytical generalized Jacobian agrees with a finite-difference approximation, with relative discrepancy 5.407×10^{-9} in the reported verification test. The spherical curvature correction was independently verified using finite differences, with a maximum reported absolute discrepancy of approximately $2.24\times10^{-13}\,\mathrm{m}$.

To quantify the influence of the additional second-order terms, the relative change in the contact-force vector is evaluated as

$$\Delta_f^{(a,b)} = 100\frac{\|\mathbf{f}^{(b)} - \mathbf{f}^{(a)}\|_2}{\|\mathbf{f}^{(a)}\|_2}, \tag{77}$$

where $\mathbf{f}$ contains the stacked normal and net tangential contact-force components. Table 2 reports the gravity-only solutions. All four satisfy the stated numerical admissibility tests, with Fischer–Burmeister residuals below 10^{-8} and equilibrium residuals below 10^{-7}. M2 is initialized from M1, M3 from M2, and M4 from M3 when the preceding iterate satisfies the convergence criterion. Accordingly, the iteration counts are not an independent measure of relative solver efficiency.

Relative changes in the stacked normal and net tangential contact-force vectors are $1.1028\times10^{-4}\%$ between M2 and M3 and $4.359\times10^{-5}\%$ between M3 and M4. Thus, for the chosen geometry and prescribed perturbations, the additional rigid-frame corrections have little effect on the computed equilibrium force distribution. This finding is specific to the present benchmark and should not be generalized to other perturbation magnitudes or contact arrangements.

Table 2: Four-model comparison for gravity-only loading.

Model	Iter.	FB residual	Eq. residual
M1	368	9.75×10^{-9}	6.89×10^{-9}
M2	52	9.75×10^{-9}	6.37×10^{-9}
M3	39	9.85×10^{-9}	6.96×10^{-9}
M4	15	9.57×10^{-9}	6.58×10^{-9}

To examine general spatial loading, the original M1–M2 comparisons under additional applied moments are retained in Table 3. M3 and M4 have not been evaluated for these loading cases in the results reported here.

Table 3: First-order and curvature-corrected results under spatial loading.

Loading	Model	Iter.	FB residual	Eq. residual
Gravity	M1	368	9.75×10^{-9}	6.89×10^{-9}
	M2	52	9.75×10^{-9}	6.37×10^{-9}
$M_x = 0.010$	M1*	1000	1.62×10^{-7}	1.43×10^{-7}
	M2	130	9.53×10^{-9}	8.44×10^{-9}
$M_y = 0.010$	M1	163	9.33×10^{-9}	6.59×10^{-9}
	M2	40	8.97×10^{-9}	6.34×10^{-9}
$M_z = 0.010$	M1*	558	9.97×10^{-7}	9.27×10^{-7}
	M2	133	9.80×10^{-9}	9.30×10^{-9}

* The prescribed FB convergence tolerance of 10^{-8} was not reached.

All M2 solutions achieve FB residuals below 10^{-8}, whereas M1 does not reach this tolerance under M_x and M_z loading, as indicated in Table 3. Since M2 is initialized from the corresponding M1 iterate, the iteration counts should not be interpreted as a direct comparison of solver efficiency.

6.2.3 Frictional state and numerical verification

The friction margin at contact i is

$$\psi_i = f_{n,i}^2 - \frac{(f_{tp,2i-1} - f_{tm,2i-1})^2}{\mu_{1,i}^2} - \frac{(f_{tp,2i} - f_{tm,2i})^2}{\mu_{2,i}^2} \geq 0,$$

where $\mathbf{f}_{tp}$ and $\mathbf{f}_{tm}$ are the nonnegative split tangential-force components. A positive margin indicates a force strictly inside the friction region; an approximately zero margin indicates an active boundary. The associated complementarity conditions are

$$\lambda_i \geq 0, \qquad \psi_i \geq 0, \qquad \lambda_i \psi_i = 0, \qquad i = 1, 2, 3.$$

For gravity-only loading, the contact forces are compressive. Contact 1 lies inside the friction boundary, whereas contacts 2 and 3 are approximately on the boundary; the corresponding friction multipliers are approximately zero for contact 1 and positive for contacts 2 and 3. Small negative friction-margin values of numerical roundoff magnitude are assessed using the specified admissibility tolerance.

Figure 5 shows the change in normal forces between the first-order and curvature-corrected gravity-only solutions.

The small residuals, contact-force feasibility, and friction-complementarity checks establish numerical consistency of the computed MNCP solutions. They do not, by themselves, establish physical accuracy of the prescribed second-order contact motion. The present example therefore serves both as a spatial equilibrium benchmark and as a controlled sensitivity test for the added curvature and rigid-frame corrections.

6.3 Sphere on a Table Subject to an External Torque

To provide an independent verification of the equilibrium, friction, and complementarity implementation, a symmetric sphere-on-table configuration is considered. Unlike the preceding free spatial grasp example, the spherical object is supported by a horizontal table. This benchmark verifies the numerical implementation

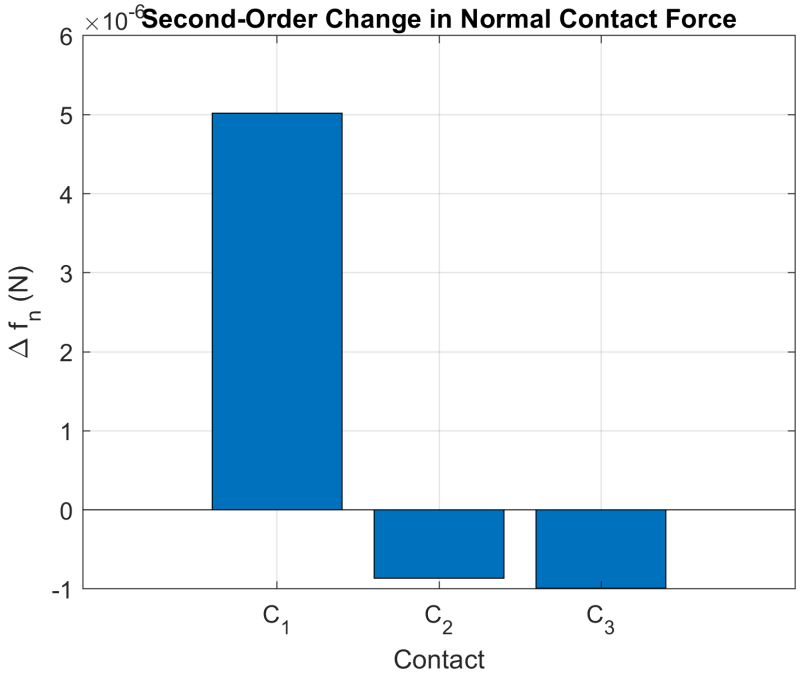


Figure 5: Normal-force changes from M1 to M2 under gravity-only loading.

against an analytically determined equilibrium configuration, rather than assessing the accuracy of the second-order geometric corrections.

A sphere of radius

$$R = 0.05 \text{ m}$$

is supported by a horizontal table and grasped by three fingers located at the polar angle

$$\theta = 60^\circ$$

and azimuth angles

$$\phi_1 = 0^\circ, \qquad \phi_2 = 120^\circ, \qquad \phi_3 = 240^\circ.$$

The configuration is illustrated in Figure 6, showing the three finger contacts, the sphere center, the applied torque, the gravitational load, and the supporting table reaction.

A pure external torque

$$\tau_z = 0.5 \text{ N m}$$

is applied about the vertical axis. The sphere weight is

$$W = 1.4715 \text{ N}.$$

For this symmetric configuration, equal azimuthal tangential forces at the three finger contacts have zero resultant force but generate a resisting moment about the vertical axis. The moment generated by each contact is

$$R \sin\theta \, f_t,$$

and moment equilibrium therefore gives

$$3R \sin\theta \, f_t = \tau_z.$$

Hence,

$$f_t = \frac{\tau_z}{3R \sin\theta} = 3.8490 \text{ N}.$$

For the analytical benchmark, a normal contact force of

$$f_n = 10 \text{ N}$$

is selected at each finger contact. This value represents a prescribed normal preload rather than a force uniquely determined by the equilibrium equations.

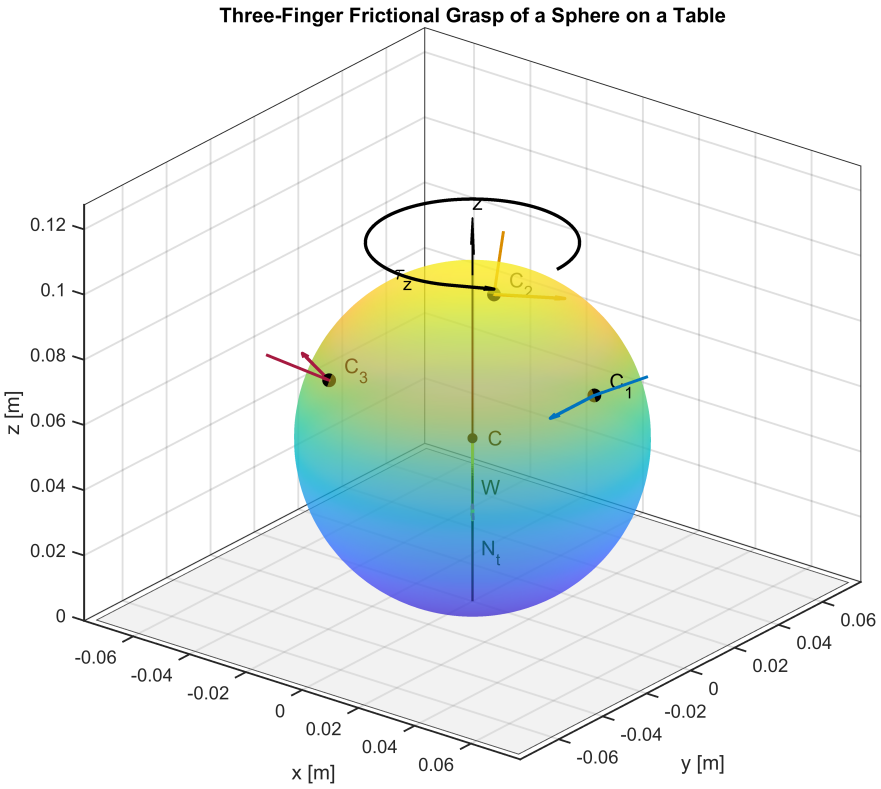


Figure 6: Three-finger frictional grasp of a sphere supported by a horizontal table.

The contact friction coefficients along the two local tangential directions are $\mu_1 = 0.5$ and $\mu_2 = 0.4$. Since the analytical resisting force acts entirely along the first tangential direction, the available friction force in that direction is

$$\mu_1 f_n = 5 \text{ N}.$$

The corresponding friction utilization is

$$\rho = \frac{f_t}{\mu_1 f_n} = 0.7698 < 1,$$

confirming that the analytical contact forces lie strictly inside the admissible friction region.

By symmetry, the horizontal components of the three normal contact forces cancel. The vertical components are balanced by the supporting table reaction and the sphere weight. Vertical equilibrium therefore gives

$$N_t = W + 3 f_n \cos\theta.$$

Substituting the benchmark parameters yields

$$N_t = 1.4715 + 3(10)\cos 60^\circ = 16.4715 \text{ N}.$$

In the numerical benchmark, this analytically determined table reaction is prescribed as an external supporting force rather than introduced as an additional contact unknown in the MNCP.

The first-order MNCP solution reproduces the analytical finger-contact forces,

$$f_n = 10.0000 \text{ N}, \qquad \|\mathbf{f}_t\| = 3.8490 \text{ N},$$

at each of the three contacts. The equilibrium residual is 6.37×10^{-12}, while the Fischer–Burmeister residual is 1.47×10^{-10}. The analytical reference equilibrium residual is 5.83×10^{-15}.

The agreement between the analytical and numerical contact forces supports the consistency of the equilibrium, friction, and complementarity implementation for the prescribed benchmark conditions. The equal normal and tangential contact-force magnitudes follow from the symmetry of the selected configuration and are not imposed by the general MNCP formulation.

The solver parameters and the sensitivity of the first-order benchmark to different initial contact-force values are summarized in Table 4.

Table 4: Solver parameters and sensitivity to initial values.

Solver parameters	
Maximum iterations	200
Convergence tolerance	10^{-9}
Regularization parameter	10^{-8}
Line-search parameter	10^{-4}
Maximum line-search steps	40
Maximum relative step	1.0

Initial scale	Iter.	FB residual	Equil. residual	Force error (N)
0.5	10	6.29×10^{-10}	2.73×10^{-11}	3.63×10^{-10}
0.8	11	1.47×10^{-10}	6.37×10^{-12}	8.50×10^{-11}
1.2	7	6.39×10^{-10}	6.13×10^{-11}	8.18×10^{-10}
1.5	13	9.78×10^{-10}	4.23×10^{-11}	5.64×10^{-10}

Four initial contact-force scales were tested, ranging from 0.5 to 1.5 times the reference values. All cases converged within 7–13 iterations, with Fischer–Burmeister residuals below 10^{-9} and contact-force errors below 10^{-9} N. These results indicate limited sensitivity to the tested initial contact-force values.

To examine the influence of second-order geometric corrections, two additional models are evaluated using prescribed perturbations. The first includes the normal curvature correction $\mathbf{\Gamma}_n$, while the second additionally includes the rigid-frame tangential correction $\mathbf{\Gamma}_t$. Both models converge with Fischer–Burmeister residuals below 10^{-9} and equilibrium residuals below 10^{-10}. The resulting changes in contact forces are small, while the corrections produce measurable differences in the predicted object displacement. These comparisons are interpreted as geometric sensitivity tests rather than independent validation of a fully coupled second-order contact model.

6.4 Discussion

The three examples demonstrate complementary aspects of the proposed formulation. The planar case shows that surface curvature generates a quadratic correction to the contact gap that grows with tangential perturbation. The spatial three-finger case shows that this correction changes the contact-force distribution enough to affect the available friction margin. The sphere-on-table benchmark confirms that the implementation reproduces the analytical equilibrium solution to within machine precision.

These examples also illustrate the distinction between numerical accuracy and physical significance. Small equilibrium and FB residuals demonstrate that the solver has found a solution of the MNCP system, but they do not by themselves establish the importance of the second-order geometry. That importance is determined instead by whether the curvature-dependent terms change the predicted proximity to incipient slip.

7 Conclusion

This work has shown that incorporating second-order contact kinematics into a complementarity formulation of frictional grasping yields a tractable extension of the standard first-order model. The resulting mixed nonlinear complementarity problem retains the unilateral and nonsmooth character of frictional contact while accounting for curvature-dependent geometric effects that are absent from a linearized description. The quadratic term $\mathbf{\Gamma}(\delta\boldsymbol{\eta}, \delta\boldsymbol{\eta})$ appears explicitly in the contact compatibility relations, and the resulting system is solved by a regularized semismooth Newton method based on the Fischer–Burmeister reformulation.

The numerical examples illustrate the influence of prescribed second-order geometric corrections on the computed contact response. The spatial three-finger case shows that second-order geometry can modify the contact-force distribution enough to change the available friction margin. The sphere-on-table benchmark provides an independent check of the equilibrium, friction, and complementarity implementation against an analytical solution.

A central observation is that the significance of the second-order terms cannot be assessed solely through changes in the numerical residual. Their principal physical effect is the coupling between relative tangential motion, local surface curvature, and the resulting contact response. In configurations where these effects are

non-negligible, neglecting the second-order terms may lead to an inaccurate assessment of the admissible frictional state, even though the first-order and second-order residuals may appear numerically similar.

The computed MNCP solution is generally local, and the semismooth Newton method used to solve it is only locally convergent. The present study is also restricted to contact-level models and does not include an explicit multi-joint hand mechanism or experimental validation. Future work will address explicit multifingered-hand kinematics, a fully coupled treatment of the tangential second-order term $\mathbf{\Gamma}_t$, and extensions to rolling contact, dynamic grasping, and experimental validation.

Data Availability

No experimental datasets were used in this study. The MATLAB code used for the numerical implementation is available from the author upon reasonable request.

CRediT authorship contribution statement

Ahmad M. Al-Fahed Nuseirat: Conceptualization, Methodology, Formal analysis, Software, Validation, Investigation, Writing – original draft, Writing – review & editing, Visualization.

Declaration of Competing Interest

The author declares that he has no known competing financial interests or personal relationships that could have appeared to influence the work reported in this paper.

Funding

This research received no specific grant from any funding agency in the public, commercial, or not-for-profit sectors.

Ethical Approval

This study does not involve human participants or animals, and therefore, ethical approval was not required.

Declaration of Generative AI and AI-Assisted Technologies

During the preparation of this work, the author used generative AI (ChatGPT, OpenAI) to assist with language refinement, organization, and readability. The author reviewed and edited the content as needed and takes full responsibility for the content of the publication.

References

[1] A. Bicchi and V. R. Kumar. Robotic grasping and contact: A review. In *Proc. of the 2000 IEEE Int. Conf. on Robot. and Autom. (ICRA)*, volume 1, pages 348–353, San Francisco, CA, 2000. https://doi.org/10.1109/ROBOT.2000.844081.

[2] J. Kerr and B. Roth. Analysis of multifingered hands. *Int. J. Robot. Res.*, 4(4):3–17, 1986. https://doi.org/10.1177/027836498600400401.

[3] A. Sahbani, S. El-Khoury, and P. Bidaud. An overview of 3D object grasp synthesis algorithms. *Robot. Auton. Syst.*, 60(3):326–336, 2012. https://doi.org/10.1016/j.robot.2011.07.016.

[4] C. Xiong, Y. Li, Y. Xiong, H. Ding, and Q. Huang. Grasp capability analysis of multifingered robot hands. *Robot. Auton. Syst.*, 27(4):211–224, 1999. https://doi.org/10.1016/S0921-8890(99)00007-X.

[5] B. Barkat, S. Zeghloul, and J.-P. Gazeau. Optimization of grasping forces in handling of brittle objects. *Robot. Auton. Syst.*, 57(4):460–468, 2009. https://doi.org/10.1016/j.robot.2008.05.004.

[6] Y. Zheng. Real-time contact force distribution using a polytope hierarchy in the grasp wrench set. *Robot. Auton. Syst.*, 99:97–109, 2018. https://doi.org/10.1016/j.robot.2017.10.014.

[7] P. D. Panagiotopoulos. *Inequality Problems in Mechanics and Applications: Convex and Nonconvex Energy Functions*. Birkhäuser, Boston, MA, 1985. https://doi.org/10.1007/978-1-4612-5152-1.

[8] J. J. Moreau and P. D. Panagiotopoulos, editors. *Nonsmooth Mechanics and Applications*, volume 302 of *CISM Courses and Lectures*. Springer-Verlag, Vienna, 1988. https://doi.org/10.1007/978-3-7091-2624-0.

[9] B. Brogliato. *Nonsmooth Mechanics: Models, Dynamics and Control*. Springer, Cham, 3rd edition, 2016. https://doi.org/10.1007/978-3-319-28664-8.

[10] D. E. Stewart and J. C. Trinkle. An implicit time-stepping scheme for rigid body dynamics with inelastic collisions and Coulomb friction. *Int. J. Numer. Methods Eng.*, 39(15):2673–2691, 1996. https://doi.org/10.1002/(SICI)1097-0207(19960815)39:15<2673::AID-NME972>3.0.CO;2-I.

[11] M. Anitescu and F. A. Potra. Formulating dynamic multi-rigid-body contact problems with friction as solvable linear complementarity problems. *Nonlinear Dynamics*, 14(3):231–247, 1997. https://doi.org/10.1023/A:1008292328909.

[12] F. Facchinei and J.-S. Pang. *Finite-Dimensional Variational Inequalities and Complementarity Problems*. Springer, New York, NY, 2003. ISBN 978-0-387-95580-3.

[13] J. S. Pang and J. C. Trinkle. Complementarity formulations and existence of solutions of dynamic multi-rigid-body contact problems with Coulomb friction. *Mathematical Programming*, 73(2):199–226, 1996. https://doi.org/10.1007/BF02592103.

[14] J. C. Trinkle. A quantitative test for form closure grasps. In *Proceedings of the IEEE/RSJ International Conference on Intelligent Robots and Systems*, pages 1670–1677, 1992. https://doi.org/10.1109/IROS.1992.594246.

[15] A. M. Al-Fahed, G. E. Stavroulakis, and P. D. Panagiotopoulos. Hard and soft fingered robot grippers: The linear complementarity approach. *Z. Angew. Math. Mech.*, 71(7/8):257–265, 1991. https://doi.org/10.1002/zamm.19910710718.

[16] A. Al-Fahed and P. D. Panagiotopoulos. A linear complementarity approach to the articulated multifingered friction gripper. *J. Robot. Syst.*, 10(6):871–887, 1993. https://doi.org/10.1002/rob.4620100606.

[17] A. M. Al-Fahed Nuseirat and G. E. Stavroulakis. A complementarity problem formulation of the frictional grasping problem. *Comput. Methods Appl. Mech. Eng.*, 190(8–10):941–952, 2000. https://doi.org/10.1016/S0045-7825(99)00454-5.

[18] F. E. Buffo and M. C. Maciel. A mixed nonlinear complementarity technique for solving the dynamics of a dexterous manipulation system. *Comput. Appl. Math.*, 25(1):79–95, 2006. https://doi.org/10.1590/S0101-82052006000100004.

[19] F. Pfeiffer and C. Glocker. *Multibody Dynamics with Unilateral Contacts*. Wiley Series in Nonlinear Science. John Wiley & Sons, New York, 1996. https://doi.org/10.1002/9783527618385.

[20] David J. Montana. The kinematics of contact and grasp. *The International Journal of Robotics Research*, 7(3):17–32, 1988. https://doi.org/10.1177/027836498800700302.

[21] C. Cai and B. Roth. On the spatial motion of a rigid body with point contact. In *Proc. IEEE Int. Conf. Robot. Autom.*, pages 686–695, Raleigh, NC, 1987. https://doi.org/10.1109/ROBOT.1987.1087971.

[22] E. Rimon and J. W. Burdick. Mobility of bodies in contact—part i: A 2nd-order mobility index for multiple-finger grasps. *IEEE Trans. Robot. Autom.*, 14(5):696–708, 1998. https://doi.org/10.1109/70.720347.

[23] E. Rimon and J. W. Burdick. Mobility of bodies in contact—part ii: How forces are generated by curvature and friction. *IEEE Trans. Robot. Autom.*, 15(5):844–857, 1999. https://doi.org/10.1109/70.795790.

[24] W. S. Howard and V. Kumar. On the stability of grasped objects. *IEEE Trans. Robot. Autom.*, 12(6): 904–917, 1996. https://doi.org/10.1109/70.544773.

[25] A. Fischer. A special Newton-type optimization method. *Optimization*, 24(3-4):269–284, 1992. https://doi.org/10.1080/02331939208843795.

[26] C. Kanzow. Some noninterior continuation methods for linear complementarity problems. *SIAM Journal on Matrix Analysis and Applications*, 17(4):851–868, 1996. https://doi.org/10.1137/S0895479894273134.

[27] C. Kanzow and D. Steck. An inexact semismooth Newton method for nonlinear complementarity problems. *Comput. Optim. Appl.*, 76(1):75–102, 2020. https://doi.org/10.1007/s10589-020-00182-z.

[28] G. E. Stavroulakis, P. D. Panagiotopoulos, and A. M. Al-Fahed. On the rigid body displacements and rotations in unilateral contact problems and applications. *Computer and Structures*, 40(3):599–614, 1991. https://doi.org/10.1016/0045-7949(91)90229-F.

[29] Richard M. Murray, Zexiang Li, and S. Shankar Sastry. *A Mathematical Introduction to Robotic Manipulation*. CRC Press, 1994.

[30] C. Chen and O. L. Mangasarian. A class of smoothing functions for nonlinear and mixed complementarity problems. *Computational Optimization and Applications*, 5:97–138, 1996. https://doi.org/10.1007/BF00249052.